EJNMMI Research

ORIGINAL RESEARCH

Open Access

A study method using early dynamic acquisition of [^{18}F]fluorodopa positron emission tomography for the differential diagnosis between progression and radionecrosis of brain metastases after radiotherapy

Ines Barrat[1], Marc-Etienne Meyer[1,2], Alexandre Coutte[3], Mathieu Boone[4], Roger Bouzerar[1] and Pascal Bailly[1,5*]

Abstract

Background It is difficult to distinguish between the brain metastasis progression (BMP) and brain radionecrosis (BRN) on the basis of ^{18}F-3,4-dihydroxyphenylalanine positron emission tomography/computed-tomography (^{18}F-FDOPA PET/CT) data. The advent of silicon photomultiplier (SiPM) PET technology makes it possible to study dynamic volumes and potentially improve diagnostic accuracy. We developed a method for processing ^{18}F-FDOPA PET/CT in the differential diagnosis between BMP and BRN. The method involves a short (3-second) sampling time during a 4-minute acquisition on a SiPM-PET/CT machine. We prospectively included 15 patients and 19 metastases. All acquisitions were performed in list mode acquisition for 25 min on a four-ring SiPM PET/CT system. We calculated the ratios between the maximum activity in the lesion's voxel and the mean activity in the contralateral region (VOImax/CLmean) or the mean activity in the white matter (VOImax/WMmean).

Results Seven lesions were classified as BMP and twelve were classified as BRN. Statistically significant intergroup differences in the VOImax/CLmean and VOImax/WMmean activity ratios were observed for both the clinical volume and the early acquisition. The best performing quantitative variable was the VOImax/CLmean ratio on early acquisition, with a diagnostic accuracy of 94.7%, a sensitivity of 100%, and a specificity of 91.7%.

Conclusion The ^{18}F-FDOPA PET/CT data acquired a few minutes after the bolus injection confirms its value in differentiating between BMP and BRN, compared to the much longer classic clinical protocol.

Keywords Brain metastasis, Progression, Radionecrosis, FDOPA PET, Dynamic acquisition

*Correspondence:
Pascal Bailly
Bailly.Pascal@chu-amiens.fr
[1]Nuclear Medicine Department, Amiens University Medical Center, Amiens, France
[2]Jules Verne University of Picardie, Amiens, France
[3]Radiotherapy Department, Amiens University Medical Center, Amiens, France
[4]Medical Oncology Department, Amiens University Medical Center, Amiens, France
[5]Service de Médecine Nucléaire, unité TEP Centre Universitaire Hospitalier Amiens – Picardie, 1 Rond-Point du Professeur Christian CABROL, Amiens cedex 80054, France

Background

The cancers most likely to cause brain metastases (BM) are primary lung cancers, followed by breast cancers and melanomas [1]. Due to the high morbidity and mortality rates associated with BM, effective screening, treatment and therapeutic monitoring are essential [2]. Various treatment options are available for BM, depending on factors such as the lesion site and the number of lesions. Surgical resection may be recommended in some cases, while radiotherapy, chemotherapy and immunotherapy are also commonly used [3]. Brain radionecrosis (BRN) is a potential complication of radiation therapy for the treatment of BM and may occur several months to years after the course of treatment [4].

The pathogenesis of BRN is poorly understood but appears to involve vasculitis, an immune reaction, and demyelination [5, 6]. Although radiation therapy is often used to treat BM, it may cause this serious complication [7]. Differentiating between BRN and BM progression (BMP) is essential for determining the appropriate treatment approach [8, 9].

Contrast-enhanced magnetic resonance imaging (MRI) is the technique most widely used to monitor BM [10]. In particular, measurement of the relative cerebral blood volume (rCBV, derived from perfusion-weighted imaging) makes it possible to differentiate between BMP and BRN [11]. In some cases, however, brain lesions may consist of a mixture of necrotic tissue and tumour progression; in such a case, differentiation between BMP and BRN is difficult on the basis of imaging alone [12]. Another diagnostic difficulty arises when the BM are located close to (and are difficult to distinguish from) large blood vessels on MRI, leading to false positive or false negative results. These limitations are driving researchers to develop additional imaging or post-processing techniques. For example, MR spectroscopy, particularly choline concentration in tissues which correlates with tumor progression, or radiomics analysis which extracts texture and shape features that characterize the tumor lesion, may be of interest. Amide proton transfer-weighted (APTw) imaging is another advanced MRI technique, in which image contrast is provided primarily by amide protons in cellular proteins and peptides, which can be used to distinguish brain metastases from glioblastoma [13]. In combination with MRI, PET imaging has also seen the development of several technological advances to assist in the differential diagnosis; however its accessibility in practice remains limited [14]. Amino-acid PET imaging is a valuable technique that complementing MRI in neuro-oncology, mainly for glioma evaluation. The most commonly studied amino-acid tracers are [11 C]-L-methyl-methionine (11 C-MET), [18F]-fluoroethyl-L-tyrosine (18F-FET) and [18F]-L-dihydroxyphenylalanine (^{18}F-FDOPA) with the second being the most prevalent in literature data on glioma diagnosis [15]. 18F-FDOPA has been studied to a lesser extent in this topic, and even less so in analyses related to brain metastases. The combined use of [18F]-L-dihydroxyphenylalanine (^{18}F-FDOPA) positron emission tomography (PET) and computed tomography (CT) can also help oncologists to differentiate between BMP and BRN. The ^{18}F-FDOPA tracer is used in this indication because of its strong uptake into the brain (linked to overexpression of the amino acid transporter type 1 by brain tumours), regardless of whether or not the blood-brain barrier is affected. The main benefit is an excellent signal-to-noise ratio [16].

Several studies of gliomas have shown that ^{18}F-FDOPA PET/CT imaging is equivalent or even superior to contrast-enhanced MRI [17, 18]. However, only a few researcher groups have investigated the use of ^{18}F-FDOPA PET/CT technique for BM imaging. Nevertheless, the results of some of these studies are promising. In particular, Cicone et al. found that the diagnostic performance was better for ^{18}F-FDOPA PET/CT than for perfusion MRI [19].

The recommended ^{18}F-FDOPA PET/CT brain protocol comprises a 15-minute post-injection tracer uptake period and a 10-minute acquisition [20].

Despite the potential benefits of ^{18}F-FDOPA PET/CT, the differential diagnosis of BMP vs. BRN remains in routine clinical practice is complicated by radiotherapy-induced changes in vascularization, perfusion, and local metabolism. Imaging solutions such as dynamic PET/CT with silicon detectors (SiPM-PET) may help to better understand the vascularization and metabolic patterns of BM and improve the accuracy of differentiation between BMP and BRN. Indeed, the latest SiPM-PET devices are more sensitive than previous generations of photomultiplier-based PET devices [21]. The high sensitivity and greater time resolution of SiPM-PET based scanners make them particularly useful for dynamic imaging studies. However, custom postprocessing software tool for the analysis of dynamic volume functions is not provide on the manufacturer's console.

The objective of the present study was to determine the differential diagnostic performance (BMP vs. BRN) of a method for processing ^{18}F-FDOPA SiPM-PET data. The method involves a short (3-second) sampling time during a 4-minute acquisition on a SiPM-PET/CT machine.

Materials and methods

Study population

The main inclusion criterion was doubt with regard to the presence of BMP vs. BRN four months after the end of radiotherapy, regardless of the type of primary tumour. All patients included in the study gave their informed

consent. Patients fasted for four hours before the imaging session and were not premedicated with carbidopa.

The final diagnosis of malignancy was determined either from histological confirmation (3 patients) or on from combination of clinical and/or radiological follow-up, up to six months after the 18 F-FDOPA PET-CT examination. Imaging follow-up did not include the method evaluated in the present study.

PET/CT acquisitions and reconstructions

All imaging data were acquired using a 4-ring whole-body SiPM-PET/CT Discovery MI system (GE Healthcare, Waukesha, WI, USA), which features a 198 mm axial and a 700 mm transaxial field of view (FOV) [22]. The acquired data (prompts) collected in a single step centered on the brain are stored in real-time in a List Mode (LM) file for 25 min, starting before the injection of ^{18}F-FDOPA (i.e. no synchronization between the start of the acquisition and the manual injection of ^{18}F-FDOPA).

All PET images in this study were reconstructed using the attenuation-weighted ordered subset expectation maximization algorithm (AW-OSEM) [23] on the manufacturer's console with attenuation correction coefficients calculated from CT low dose acquisitions (120 kV, 60 mA, and 511 keV). The AW-OSEM algorithm's reconstruction parameters were set to 2 iterations, 17 subsets, a matrix size of 256×256 voxels, 71 slices, a useful FOV reconstruction diameter of 30 cm (i.e. a voxel size of 1.17 mm x 1.17 mm x 2.79 mm), 4-mm Gaussian filter with point spread function, decay, scatter and attenuation correction.

Clinical volume

To replicate the ^{18}F-FDOPA PET examination conducted in routine clinical practice we only analyzed data from the last 10 min of the LM file (Fig. 1).

4D-stack volume

The LM file enabled us to generate 80 volumes, forming a four-dimensional (4D) stack. Each volume corresponded to a period of 3 s during the initial 4 min of the acquisition (Fig. 1).

3D-sum volume

Our in-house tool, described in the following paragraph, includes T0 computation and the summation of multiple volumes, enabling us to generate a volume referred to as the 3D summation volume (3D-sum) (Fig. 2). This approach is intended to enhance the contrast and corresponds to the time-domain integration of specific volumes within the 4D-stack. 3D-sum was computed for each patient and thus summarizes the 4D-stack volumes from volume T0+20 to volume T0+30, as explained and discussed below (see Fig. 2).

Development of an in-house MATLAB software tool

We used MATLAB software (2023b, The MathWorks Inc., Natick, MA, USA) to develop a custom software called 'Visu-Stack' (VS). This software enabled us to study dynamic volume functions that are not accessible with the manufacturer's console (VS interface is provided in the Supplementary Materials). VS uses reconstructions from the manufacturer's console. It also applied a time filter to all the 4D-stack data in this study by convolution array of low-pass form as $\frac{1}{3}[1\ 1\ 1]$.

Due to the lack of synchronisation between the acquisition and the injection, we had to determine the time at which the ^{18}F-FDOPA bolus arrived in the camera's Field of view (FOV). Thus, VS determined the volume number (T0) of the 4D-stack, which indicates the arrival time. T0 corresponded to the index of the volume within the 4D-stack reconstructed with as many prompt events as possible Furthermore, VS included a function that

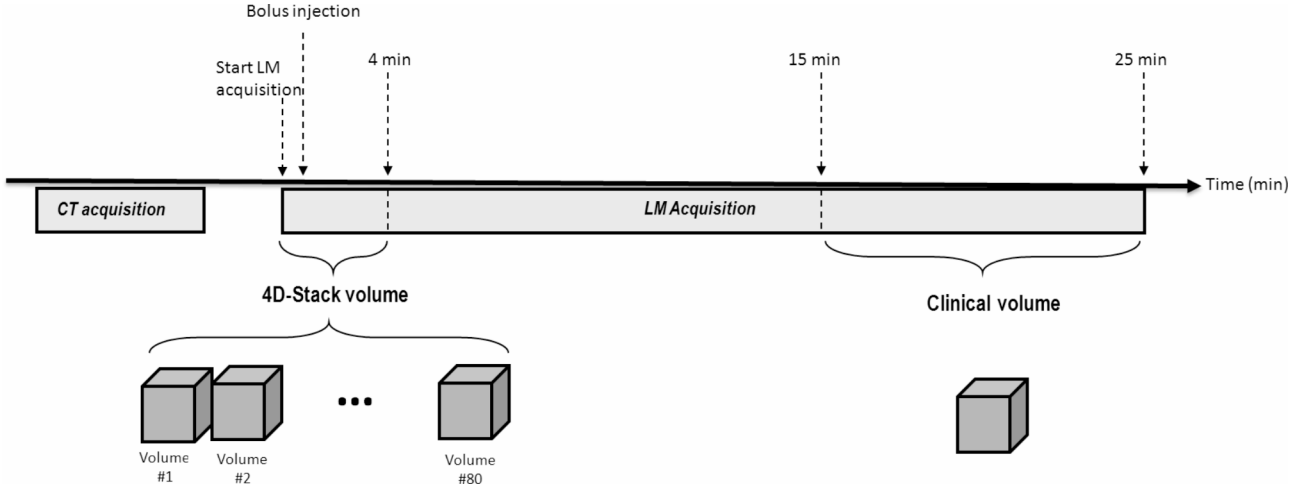

Fig. 1 A schematic depiction of the timeline for CT acquisition, PET/CT acquisition, and radiotracer injection, and an overview of the generation of the 4D-stack and clinical volumes used in this study

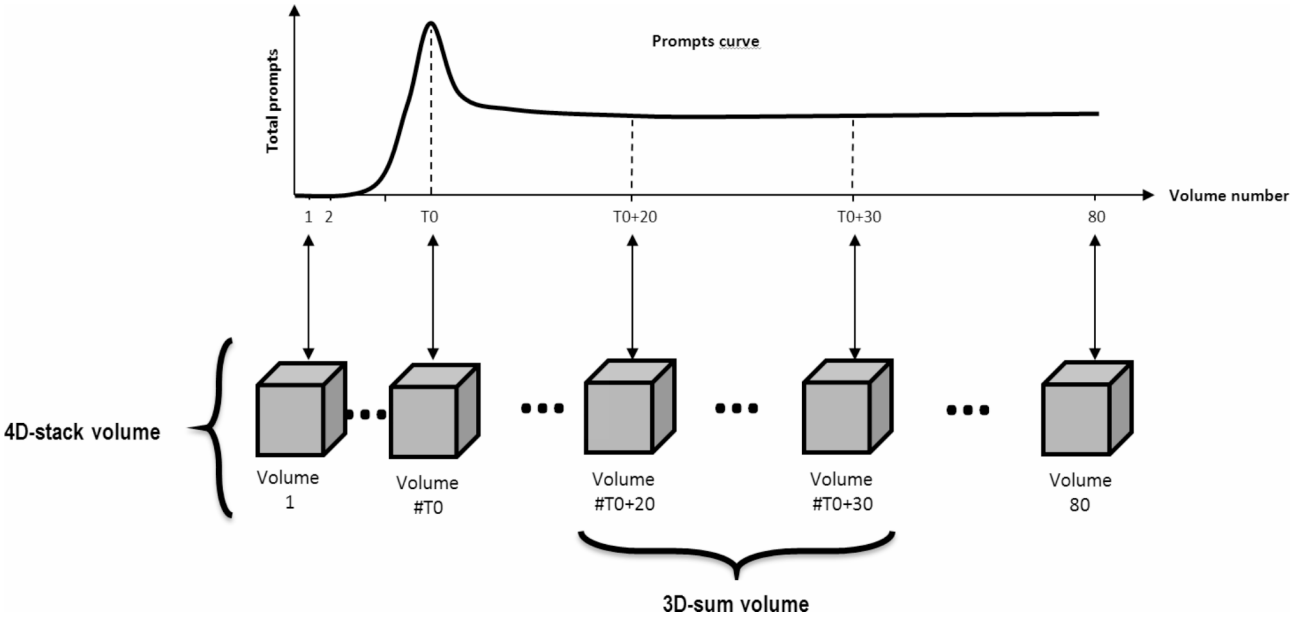

Fig. 2 A block diagram for creation of the 3D-sum volume from the T0 value and the 4D-stack volume

generates a single volume by voxel-by-voxel summation of multiple volumes. VS also generates a time-activity curve (TAC) and calculates the mean of a set of TACs (TAC_{mean}), based on the 4D-stack.

Lastly, the VS implementation includes 3D measurements, such as identifying the maximum value and its corresponding coordinates within a spherical region of interest (VOI_max) and calculating the mean value within a circular region of interest (ROI_mean).

Measurements and analyses

For all the patients in this study, the mean activity in the ROI (with a diameter of 5 voxels) was measured in the contralateral region ($\boldsymbol{CL}_{mean}$) and in white matter ($\boldsymbol{WM}_{mean}$) [24] for both the clinical volume (Fig. 1) and the 3D-sum volume. Furthermore, a VOI encompassing the lesion was measured in both the clinical and 3D-sum volumes to determine the maximum voxel activity within the lesion ($\boldsymbol{VOI}_{max}$).

These measurements allowed us to calculate the ratios $\boldsymbol{VOI}_{max}/\boldsymbol{CL}_{mean}$ and $\boldsymbol{VOI}_{max}/\boldsymbol{WM}_{mean}$ for both the clinical and 3D-sum volumes.

Statistical analysis

Categorical variables were reported as the frequency (percentage), and quantitative variables were reported as the median [interquartile range (IQR)]. Means of continuous variables were compared in the Mann-Whitney U test. Diagnostic performance was assessed using a receiver-operating characteristic curve analysis, with maximization of Youden's index. The sensitivity, specificity, accuracy and the area under the curve (AUC) were calculated. All statistical analyses were performed using Rstudio software (version 1.3.1093 (Rv.3.6.3, http://www.r-project.org). The threshold for statistical significance was set to $p<0.05$.

Results

Study population

Fifteen patients with a total of 19 lesions were included in the study (Table 1). Two patients with two brain lesions were analyzed and two patients with only one lesion were studied twice. None of the lesions were located close to the striatum. According to the diagnostic gold standard, seven lesions were classified as BMP and 12 were classified as BRN. All metastasis were irradiated (median [IQR] total dose: 30 Gy [24–33] and 3 lesions (16%) were removed surgically before radiation treatment. Sixteen patients were treated with stereotactic radiotherapy (SRT), two patients with stereotactic radiosurgery (SRS) and one patient with both SRS and whole-brain radiation therapy (WBRT). The median [IQR] time interval between the end of radiotherapy and the ^{18}F-FDOPA PET/CT examination was 14 months [11–34].

The median ^{18}F-FDOPA activity injected was 121 MBq (117–136), which corresponds to a median concentration of 1.9 MBq/kg (1.8-2.0).

Quantitative analysis of the clinical and 3D-sum volumes

Inside the regions of interest, statistically significant differences between BMP and BRN groups were observed for all the variables studied (Fig. 3; Table 2). The clinical images, the 3D-sum images in a patient with both BMP and BRN are shown in Fig. 4.

Table 1 Demographic and baseline clinical characteristics of the study population

Overall study population (*n* = 15)	
Sex	
Men	6
Women	9
Primary tumor	
Lung	7 (47%)
Breast	3 (20%)
Melanoma	2 (13%)
Kidney	1 (7%)
Undetermined	2 (13%)
Metastasis site	
Supratentorial	11 (73%)
Infratentorial	4 (27%)
Histological diagnosis	3 (20%)
BMI (kg/m^2)	27 (25–29)
Age (years)	73 (62–76)
Time interval between MRI and PET (days)	42 (20–56)
Type of Radiation therapy	
SRT	16 (84%)
SRS	2 (11%)
WBRT and SRS	1 (5%)
Radiation total dose (Gy)	
SRT	27 (24–33)
SRS	29 (26–31)
WBRT and SRS	57
Total number of lesions	19

BMI : body mass index ; SRT : stereotactic radiotherapy ; SRS : stereotactic radiosurgery ; WBRT : whole-brain radiation therapy

Assessment of diagnostic performance

The best performances were found for the 3D-sum volume, which gave an accuracy of 94.7% for both contralateral normalization and white matter normalization (Table 3). Furthermore, the highest AUC value (0.99) was observed for the contralateral normalization in the 3D-sum volume, with 100% sensitivity and only one false positive reported whereas only one false negative was observed when using the white matter normalization. The false positive case occurred in a 77- year-old patient with primary bronchopulmonary adenocarcinoma. He received a total dose of 30 Gy in 3 fractions for his brain lesion which was located in the left occipital region and the delay between the end of radiotherapy and the PET exam was 1813 days. The false negative case occurred in a 73-year-old patient with primary renal carcinoma. He received a total dose of 30 Gy in 3 fractions for his brain lesion which was located in the right temporal area and the delay between the end of radiotherapy and the PET exam was 288 days. These two patients did not benefit from histological diagnosis and were diagnosed from clinical-radiological follow-up by a multidisciplinary committee.

The performances observed for the clinical volume were slightly lower, with accuracies of 84.2% and 89.5% accuracy for the CL and WM ratios, respectively.

Discussion

With the increasing use of radiotherapy for the treatment of BM, it is necessary to accurately differentiate between BRN and BMP during follow-up because the treatment modalities are radically different. The imaging presentations of BRN and BMP are sometimes similar. Hence, the objective of the present study was to improve the differential diagnosis by applying a method for processing ^{18}F-FDOPA PET/CT data. This method involves a short (3-second) sampling time during a 4-minute acquisition on a SiPM-PET machine. In order to efficiently exploit the dynamic images, we have specifically developed a custom MATLAB post-processing tool (VS) not available on the manufacturer's console.

The latest generation of SiPM-PET machines provides greater detection sensitivity. We harnessed these capabilities for data acquired over a short (3-second) period. Moreover, each volume was obtained with 3D reconstruction (i.e. spatial Gaussian post filtering). This method was only optimal for clinical volumes. We therefore incorporated time-domain filtering into VS and applied it to all 4D-stacks in our study; this feature was not available on the manufacturer's console. Furthermore, we generated a summed volume (3D-sum) to enhance the contrast and enable interpretation with a single volume. The value of T0 was adjusted for each patient, due to the lack of synchronization between the manual start of the LM acquisition and the manual injection of the bolus.

The data from our quantitative analysis are in line with the results published by Cicone et al. [19]. In the latter study, the maximum tumour activity ratio (normalized against healthy brain parenchyma, using a threshold of 1.59) allowed the diagnosis of BMP with a sensitivity of 90% and a specificity of 92%. In our study, the BRN and BMP groups differed significantly with regard to the VOI_{max}/CL_{mean} ratio for each volume (i.e. the clinical PET volume and 3D-sum). The VOI_{max}/CL_{mean} variable also gave excellent performance for just 4 min of acquisition, with a sensitivity of 85.7% and a specificity of 83.3% for the clinical PET volume and a sensitivity of 100% and a specificity of 91.7% for the 3D-sum volume.

The VOI_{max}/WM_{mean} variable has not been studied elsewhere. It also showed a good level of diagnostic performance, with a significant intergroup difference for the clinical volume and the 3D-sum volume.

We initially decided not to analyze a quantitative parameter normalized against contralateral striatal activity, given its poorer reported performance in the literature [19]. There was also a risk of bias when taking striatal

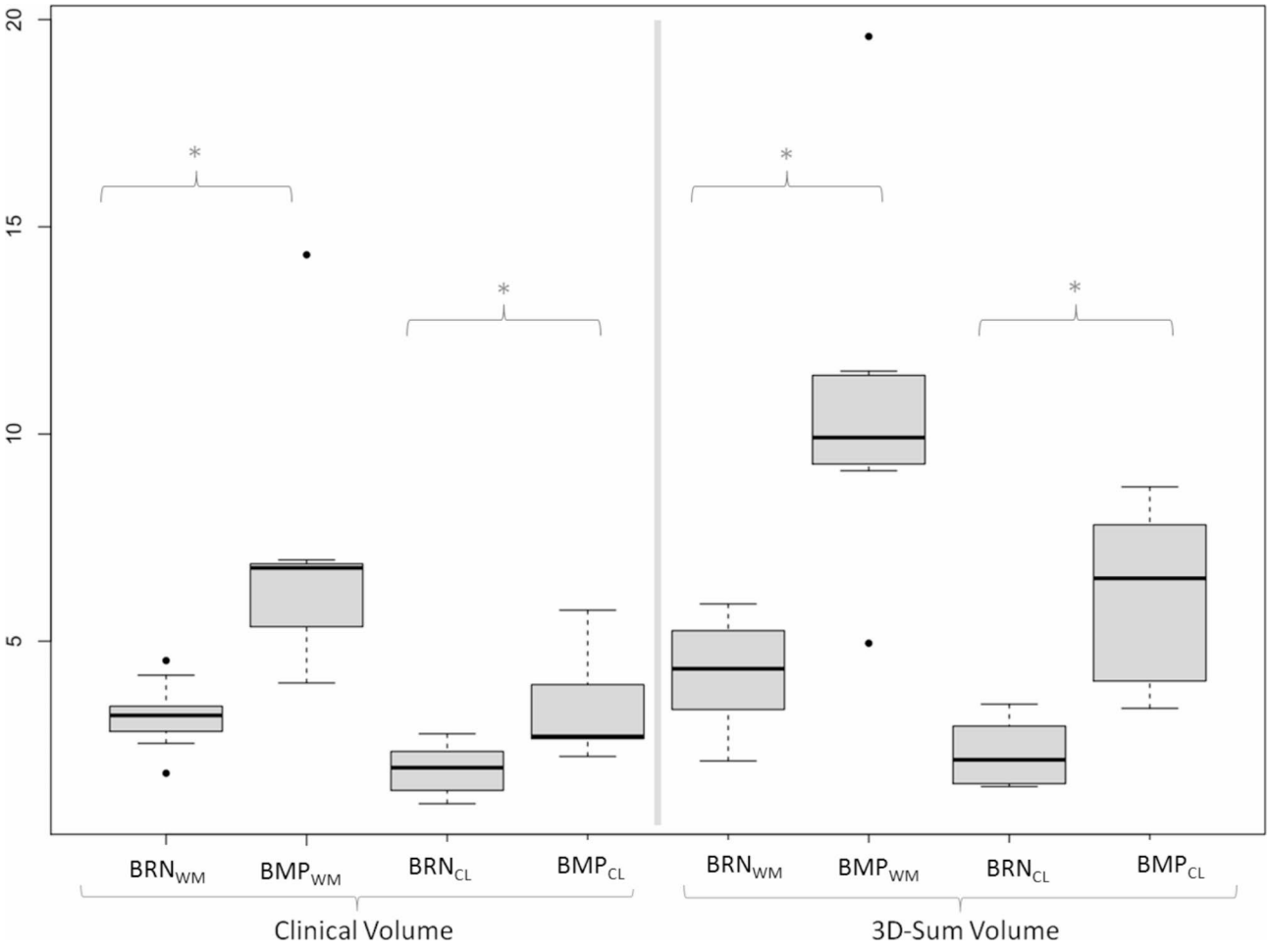

Fig. 3 Boxplot representations of ^{18}F-FDOPA uptake measurements for the BRN and BMP groups of clinical and 3D-sum volumes. WM and CL refer to the VOImax/WMmean and VOImax/CLmean ratios, respectively. The asterisk indicates a statistically significant difference

Table 2 ^{18}F-FDOPA ratio measurements for the clinical and 3D-sum volumes in the BRN and BMP groups

PET volume	Parameter	Group	Median [IQR]	Difference [95%CI]
Clinical	VOI_{max}/CL_{mean}	BRN	1.95 [1.46; 2.34]	1.13* [0.34;2.81]
		BMP	2.70 [2.65; 3.95]	
	VOI_{max}/WM_{mean}	BRN	3.21 [2.89; 3.36]	3.48** [1.30;4.24]
		BMP	6.77 [5.35; 6.87]	
3D-sum	VOI_{max}/CL_{mean}	BRN	2.14 [1.58; 2.91]	3.98** [1.70;5.78]
		BMP	6.52 [4.04; 7.81]	
	VOI_{max}/WM_{mean}	BRN	4.34 [3.46; 5.01]	5.81** [4.01;7.94]
		BMP	9.91 [9.27; 11.41]	

Note : *: $p<0.05$, **: $p<10^{-3}$

CI: confidence interval; IQR: interquartile range

activity as a reference because dopaminergic depletion is often present in the nigrostriatal pathways after radiotherapy.

In the study by Lizarraga et al. [25], the statistical performance of a 4-point visual scale for striatal activity was worse (sensitivity: 81%; specificity: 84%) than for all the quantitative variables analyzed in our study.

To the best of our knowledge, the present study is the first to have applied early-phase dynamic ^{18}F-FDOPA PET/CT analysis with a short sampling time to the differential diagnosis of BRN vs. BMP. However, many studies with amino-acid PET tracers have highlighted the value of dynamic analyses in the characterization of glial lesions [15]. Zaragori et al. showed that the slope of the

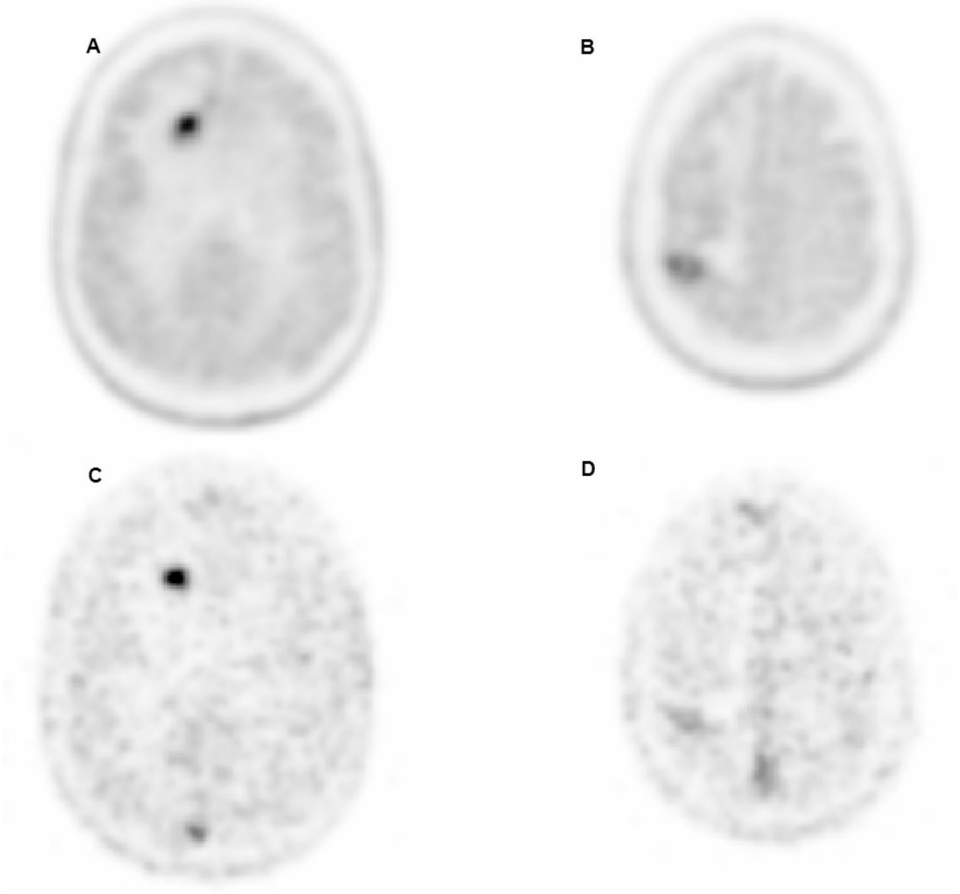

Fig. 4 ^{18}F-FDOPA PET/CT images from a patient with two lesions. The top and bottom lines show the clinical volume and 3D-sum images, respectively. The patient presented with BMP (**a, c**) and BRN (**b, d**). The values of the VOImax/CLmean ratio were (**a**) 4.79, (**b**) 2.77, (**c**) 8.73 and (**d**) 2.69

Table 3 Diagnostic performance of the quantitative variables for the clinical and 3D-sum volumes

PET volume	Variable	Cut-off	Sens (%)	Spec (%)	Accuracy	AUC
Clinical	VOI_{max}/CL_{mean}	2.64	85.7	83.3	84.2	0.89
	VOI_{max}/WM_{mean}	3.99	100	83.3	89.5	0.95
3D-sum	VOI_{max}/CL_{mean}	3.38	100	91.7	94.7	0.99
	VOI_{max}/WM_{mean}	9.11	85.7	100	94.7	0.96

Note : Sens: sensitivity; Spec: specificity; AUC: area under the curve

curve in a dynamic analysis was a predictive factor in the differential diagnosis between glioma progression and radionecrosis using ^{18}F-FDOPA PET/CT [26]. In their ^{18}F-FDOPA PET/CT study, Ceccon et al. observed a clear increase in specificity when they combined kinetic data with a quantitative analysis of the slope of the TAC in the late uptake phase 20 to 50 min after injection (93%, vs. 88% for the usual method) [27]. This observation confirmed the value of dynamic analysis, as demonstrated in our study by the activity ratios obtained from the 3D-sum volume. The software developed specifically for our study made a detailed analysis possible; today's consoles cannot perform this type of image post-processing on dynamic volumes.

Our prospective study had several limitations. Firstly, the sample size (19 lesions analyzed) was small, which reduces the power of our study. Secondly, our diagnostic gold standard (combining clinical and MRI follow-up data) has a limitation because BRN and BMP can coexist within the same lesion. Ideally, targeted biopsies or surgery should be performed on the suspected region of progression, so that reliable histological evidence and a more robust gold standard could be applied. However, the risk-benefit ratio of biopsies or surgery in each patient is low, and so this approach would not have been ethically feasible.

Our promising, preliminary results must now be confirmed in a prospective study of a larger patient population. A comparative study of the BRN and BMP TACs

derived from the first 4 min of acquisition would be interesting. Given the excellent performance of the early-phase dynamic analysis (probably due to the effects of tissue vascularization, rather than metabolism alone), it would also be interesting to perform a similar study with a less expensive 2-deoxy-2-[^{18}F]fluoro-D-glucose (^{s}F-FDG) tracer used in routine clinical practice.

Conclusion

By using a custom MATLAB software tool for post-processing, we confirmed the potential value of dynamic analysis of ^{18}F-FDOPA PET/CT data acquired just a few minutes after bolus injection in the differential diagnosis of BRN and BMP.

Abbreviations

BM	Brain metastases
BRN	Brain radionecrosis
BMP	Brain metastases progression
^{18}F-FDOPA	[18F]-L-dihydroxyphenylalanine

Supplementary Information

The online version contains supplementary material available at https://doi.org/10.1186/s13550-024-01158-7.

Supplementary Material 1

Acknowledgements

None.

Author contributions

Experimental design: IB, PB, RB, MEM.; Implementation, patient recruitment: AC, MB, IB.; Pathology diagnosis: IB, MEM, AC, MB.; Software development: PB.; Image analysis: IB, RB, PB.; Supervision: MEM.; Manuscript draft: IB, RB, PB.; Manuscript draft reviewing: IB, MEM, AC, MB, RB, PB.; All authors have read and approved the final version of the manuscript.

Funding

None.

Data availability

The datasets used and/or analyzed during the current study are available from the corresponding author on reasonable request.

Declarations

Consent for publication

All data presented have been approved for publication, each patient included in the study gave their informed consent.

Competing interests

The authors declare that they have no competing interests.

Ethical approval and consent to participate

All procedures performed in studies involving human participants were accordance with the ethical standards as laid down in the 1964 Declaration of Helsinki and its later amendments or comparable ethical standards. This prospective study was approved by an independent ethics committee (Comité de Protection des Personnes Nord-Ouest IV, Lille, France; reference 2022-A00930-43). Written informed consent was obtained from all patients. The study was registered on February 28, 2023, at ClinicalTrials.gov (NCT05762172).

Received: 30 July 2024 / Accepted: 29 September 2024

Published online: 09 October 2024

References

1. Eichler AF, Chung E, Kodack DP, Loeffler JS, Fukumura D, Jain RK. The biology of brain metastases-translation to new therapies. Nat Rev Clin Oncol. 2011;8:344–56. https://doi.org/10.1038/nrclinonc.2011.58.
2. Soffietti R, Abacioglu U, Baumert B, Combs SE, Kinhult S, Kros JM, et al. Diagnosis and treatment of brain metastases from solid tumors: guidelines from the European Association of Neuro-Oncology (EANO). Neuro Oncol. 2017;19:162–74. https://doi.org/10.1093/neuonc/now241.
3. Soffietti R, Cornu P, Delattre JY, Grant R, Graus F, Grisold W, et al. EFNS guidelines on diagnosis and treatment of brain metastases: report of an EFNS Task Force. Eur J Neurol. 2006;13:674–81. https://doi.org/10.1111/j.1468-1331.2006.01506.x.
4. Kohutek ZA, Yamada Y, Chan TA, Brennan CW, Tabar V, Gutin PH, et al. Long-term risk of radionecrosis and imaging changes after stereotactic radiosurgery for brain metastases. J Neurooncol. 2015;125:149–56. https://doi.org/10.1007/s11060-015-1881-3.
5. Nonoguchi N, Miyatake S, Fukumoto M, Furuse M, Hiramatsu R, Kawabata S, et al. The distribution of vascular endothelial growth factor-producing cells in clinical radiation necrosis of the brain: pathological consideration of their potential roles. J Neurooncol. 2011;105:423–31. https://doi.org/10.1007/s11060-011-0610-9.
6. Tanino T, Kanasaki Y, Tahara T, Michimoto K, Kodani K, Kakite S, et al. Radiation-induced microbleeds after cranial irradiation: evaluation by phase-sensitive magnetic resonance imaging with 3.0 tesla. Yonago Acta Med. 2013;56:7–12.
7. Andruska N, Kennedy WR, Bonestroo L, Anderson R, Huang Y, Robinson CG, et al. Dosimetric predictors of symptomatic radiation necrosis after five-fraction radiosurgery for brain metastases. Radiother Oncol. 2021;156:181–7. https://doi.org/10.1016/j.radonc.2020.12.011.
8. Barisano G, Bergamaschi S, Acharya J, Rajamohan A, Gibbs W, Kim P, et al. Complications of Radiotherapy and Radiosurgery in the brain and spine. Neurographics. 2011;8:167–87. https://doi.org/10.3174/ng.1700066.
9. Chao ST, Ahluwalia MS, Barnett GH, Stevens GH, Murphy ES, Stockham AL, et al. Challenges with the diagnosis and treatment of cerebral radiation necrosis. Int J Radiat Oncol Biol Phys. 2013;87:449–57. https://doi.org/10.1016/j.ijrobp.2013.05.015.
10. Tong E, McCullagh KL, Iv M. Advanced Imaging of Brain metastases: from augmenting visualization and improving diagnosis to evaluating treatment response. Front Neurol. 2020;11:270. https://doi.org/10.3389/fneur.2020.00270.
11. Wang B, Zhao B, Zhang Y, Ge M, Zhao P, Na S. at al. Absolute CBV for the differentiation of recurrence and radionecrosis of brain metastases after gamma knife radiotherapy: a comparison with relative CBV. Clin Radiol. 2018;73:758.e751-758e757 https://doi.org/10.1016/j.crad.2018.04.006
12. Kumar AJ, Leeds NE, Fuller GN, Van Tassel P, Maor MH, Sawaya RE, et al. Malignant gliomas: MR imaging spectrum of radiation therapy- and chemotherapy-induced necrosis of the brain after treatment. Radiology. 2000;217:377–84. https://doi.org/10.1148/radiology.217.2.r00nv36377.
13. Nichelli L, Casagranda S. Current emerging MRI tools for radionecrosis and pseudoprogression diagnosis. Curr Opin Oncol. 2021;33:597–607. https://doi.org/10.1097/CCO.0000000000000793.
14. Hojjati M, Badve C, Garg V, Tatsuoka C, Rogers L, Sloan A, et al. Role of FDG-PET/MRI, FDG-PET/CT, and dynamic susceptibility contrast Perfusion MRI in differentiating Radiation Necrosis from Tumor recurrence in Glioblastomas. J Neuroimaging. 2018;28:118–25. https://doi.org/10.1111/jon.12460.
15. Verger A, Imbert L, Zaragori T. Dynamic amino-acid PET in neuro-oncology: a prognostic tool becomes essential. Eur J Nucl Med Mol Imaging. 2014;48:4129–32. https://doi.org/10.1007/s00259-021-05530-w.
16. Calabria F, Chiaravalloti A, Di Pietro B, Grasso C, Schillaci O. Molecular imaging of brain tumors with 18F-DOPA PET and PET/CT. Nucl Med Commun. 2012;33:563–70. https://doi.org/10.1097/MNM.0b013e328351d566.
17. Karunanithi S, Sharma P, Kumar A, Khangembam BC, Bandopadhyaya GP, Kumar R, et al. Comparative diagnostic accuracy of contrast-enhanced MRI and (18)F-FDOPA PET-CT in recurrent glioma. Eur Radiol. 2013;23:2628–35. https://doi.org/10.1007/s00330-013-2838-6.
18. Youland RS, Pafundi DH, Brinkmann DH, Lowe VJ, Morris JM, Kemp BJ, et al. Prospective trial evaluating the sensitivity and specificity of 3,4-dihydroxy-6-[18F]-fluoro-L-phenylalanine (18F-DOPA) PET and MRI in patients with

recurrent gliomas. J Neurooncol. 2018;137:583–91. https://doi.org/10.1007/s11060-018-2750-7.
19. Cicone F, Minniti G, Romano A, Papa A, Scaringi C, Tavanti F, et al. Accuracy of F-DOPA PET and perfusion-MRI for differentiating radionecrotic from progressive brain metastases after radiosurgery. Eur J Nucl Med Mol Imaging. 2015;42:103–11. https://doi.org/10.1007/s00259-014-2886-4.
20. Law I, Albert NL, Arbizu J, Boellaard R, Drzezga A, Galldiks N, et al. Joint EANM/EANO/RANO practice guidelines/SNMMI procedure standards for imaging of gliomas using PET with radiolabelled amino acids and [(18)F]FDG: version 1.0. Eur J Nucl Med Mol Imaging. 2019;46:540–57. https://doi.org/10.1007/s00259-018-4207-9.
21. Wagatsuma K, Miwa K, Sakata M, Oda K, Ono H, Kameyama M, et al. Comparison between new-generation SiPM-based and conventional PMT-based TOF-PET/CT. Phys Med. 2017;42:203–10. https://doi.org/10.1016/j.ejmp.2017.09.124.
22. Zeimpekis KG, Kotasidis FA, Huellner M, Nemirovsky A, Kaufmann PA, Treyer V. NEMA NU 2-2018 performance evaluation of a new generation 30-cm axial field-of-view Discovery MI PET/CT. Eur J Nucl Med Mol Imaging. 2022;49:3023–32. https://doi.org/10.1007/s00259-022-05751-7.
23. Hudson HM, Larkin RS. Accelerated image reconstruction using ordered subsets of projection data. IEEE Trans Med Imaging. 1994;13:601–9. https://doi.org/10.1109/42.363108.
24. Chondrogiannis S, Marzola MC, Al-Nahhas A, Venkatanarayana TD, Mazza A, Opocher G, D, et al. Normal biodistribution pattern and physiologic variants of 18F-DOPA PET imaging. Nucl Med Commun. 2013;34:1141–9. https://doi.org/10.1097/MNM.0000000000000008.
25. Lizarraga KJ, Allen-Auerbach M, Czernin J, DeSalles AA, Yong WH, Phelps ME, et al. (18)F-FDOPA PET for differentiating recurrent or progressive brain metastatic tumors from late or delayed radiation injury after radiation treatment. J Nucl Med. 2014;55:30–6. https://doi.org/10.2967/jnumed.113.121418.
26. Zaragori T, Ginet M, Marie PY, Roch V, Grignon R, Gauchotte G, et al. Use of static and dynamic [(18)F]-F-DOPA PET parameters for detecting patients with glioma recurrence or progression. EJNMMI Res. 2020;10:56. https://doi.org/10.1186/s13550-020-00645-x.
27. Ceccon G, Lohmann P, Stoffels G, Judov N, Filss CP, Rapp M, et al. Dynamic O-(2-18F-fluoroethyl)-L-tyrosine positron emission tomography differentiates brain metastasis recurrence from radiation injury after radiotherapy. Neuro Oncol. 2017;19:281–8. https://doi.org/10.1093/neuonc/now149.

Publisher's note